Collaborative optimization of velocity planning and energy management for fuel cell hybrid buses at multiple intersections and bus stations

Energy 326 (2025) 135912

Contents lists available at ScienceDirect

Energy

journal homepage: www.elsevier.com/locate/energy

Collaborative optimization of velocity planning and energy management for fuel cell hybrid buses at multiple intersections and bus stations

Xiaohua Wu [a,b,*], Pengfei Ma [a], Lingxue Zhou [a], Zhanfeng Fan [c], Qingbo Zhu [d], Xiaofeng Yin [a], Quan Ouyang [e]

[a] Vehicle Measurement Control and Safety Key Laboratory of Sichuan Province, Sichuan Engineering Research Center of Intelligent Control and Simulation Test Technology for New Energy Vehicles, School of Automobile and Transportation, Xihua University, Chengdu, 610039, China
[b] Yibin Institute in Xihua University, Yibin, 644000, China
[c] School of Architecture and Civil Engineering, Chengdu University, Chengdu, 610106, China
[d] Department of Electrical Engineering, Chalmers University of Technology, Gothenburg, 41296, Sweden
[e] College of Automation Engineering, Nanjing University of Aeronautics and Astronautics, Nanjing, 211100, China

ARTICLE INFO

Keywords:
Fuel cell hybrid bus
Velocity planning
Energy management
Traffic light
Eco-driving
Multiple intersections

ABSTRACT

With the rapid advancement of intelligent transportation systems, a unique opportunity has emerged for optimizing energy management for hybrid electric vehicle. This paper presents a collaborative optimization method that integrates velocity planning and energy management for fuel cell hybrid buses (FCHBs) at multiple intersections and bus stations. First, an energy-saving velocity planning strategy (EVPS) is developed based on minimizing equivalent hydrogen consumption. EVPS exhibits significant advantages with respect to time savings, stopping duration, time savings rate, and overall pass efficiency at signalized intersections compared to real-based driving scenarios and modified intelligent driver model-based velocity planning strategies. Furthermore, a Q-learning-based energy management strategy (EMS) is proposed to enhance the energy efficiency and longevity of power sources in FCHBs. The EVPS is seamlessly integrated with the Q-learning-based EMS to facilitate eco-driving for the FCHBs. Finally, the effectiveness of this collaborative approach combining EVPS and EMS is experimentally validated through three real demonstration drive cycles involving FCHBs. The results indicate that the proposed EVPS-based EMS can achieve an impressive reduction in equivalent hydrogen consumption by over 21.35%.

1. Introduction

Fuel cell vehicles (FCVs) are recognized as one of the primary means to promote high-quality development within the green energy sector while addressing global climate change challenges. However, obstacles such as high hydrogen costs and complex urban traffic conditions present significant challenges to effective energy management strategies (EMSs) for FCVs [1,2]. The continually changing dynamics within urban road networks, such as variations in road slope, alterations in intersection signaling, and fluctuations in traffic flow, have a substantial impact on fuel consumption and driving times for FCVs [3,4].

With the advancement of vehicle-to-vehicle and vehicle-to-infrastructure technologies, ecological driving technologies have emerged, emphasizing the optimization of driving behavior to minimize fuel consumption and emissions. In complex urban transportation environments, the coordinated control of velocity planning strategies (VPS) and EMS has been recognized as an effective method for optimizing energy consumption, reducing vehicle idle time, and extending the lifespan of power systems [5–7]. However, many current studies overlook road infrastructure elements such as intersections, traffic signals, and bus stations encountered during actual driving scenarios. This oversight may lead to frequent starting and stopping of buses, resulting in excessive energy consumption. Therefore, investigating the impact of traffic information on vehicle driving status and developing appropriate EMSs represent a novel approach to further enhancing the fuel economy of FCVs.

An increasing number of researchers are focusing on velocity planning combined with optimal EMS to reduce energy consumption in complex traffic environments. The relationship between traffic signal information and electric vehicles (EVs) energy consumption has been explored to decrease overall energy usage while optimizing efficiency at signalized intersections [8]. To address uncertain traffic light timing, a data-driven chance-constrained eco-driving approach for

* Corresponding author.
E-mail address: xiaohuawu13@163.com (X. Wu).

https://doi.org/10.1016/j.energy.2025.135912
Received 12 February 2025; Received in revised form 23 March 2025; Accepted 29 March 2025
Available online 7 April 2025

internal combustion engine (ICE) vehicles was formulated in [9]. By considering cruise control tasks alongside acceleration characteristics parameters, an eco-driving control strategy for EVs was developed to achieve an optimized velocity profile that minimized energy consumption [10]. A two-layer model predictive control (MPC) algorithm was employed to tackle both velocity planning and power allocation challenges for hybrid electric vehicles (HEVs), thereby alleviating computational burdens [11]. Additionally, a deep deterministic policy gradient (DDPG)-based EMS for plug-in HEVs was designed by integrating signal phase timing with passenger onboard information from traffic simulations to predict optimal velocities effectively [12]. A learning-based hierarchical cooperative eco-driving with real-time traffic flow prediction was introduced for HEVs [13]. A real time multi-objective optimization Guided-MPC strategy was proposed for power-split hybrid electric buses based on velocity prediction [14].

Previous studies have investigated VPSs and EMSs for ICE vehicles, EVs, HEVs, and plug-in HEVs under various conditions. Notably, the primary power source of a FCV is the fuel cell system (FCS), whose output characteristics differ significantly from those of ICEs and batteries [15]. Therefore, a customized control strategy for FCVs is essential. A co-optimization method combining dynamic programming (DP)-based velocity planning with an alternating direction method of multipliers algorithm for energy management in FCVs navigating multiple continuous signal intersections was proposed [16]. The results indicated that this approach could achieve fuel efficiency comparable to offline DP within a real-time framework. Additionally, a long short-term memory algorithm alongside a decentralized MPC framework was introduced to optimize energy management for FCVs addressing complex and variable road conditions [17]. Another decentralized MPC based on the consensus-based alternating direction method of multipliers was proposed that explicitly considered the coordination of the dynamic reactions of the powertrain components and future driving profiles to improve the performance of FCVs [18]. Based on the health status of the FCS, an eco-driving framework utilizing DDPG algorithm under adaptive cruise control for FCVs was discussed [19]. The equivalent hydrogen consumption of this method is 94.16% of that of the DP strategy, while 19.95% reduction in health degradation. Similarly, considering future passenger number and vehicle speed [20], future terrain information [21], or environmental and look-ahead road information [22], the EMS based on DDPG for fuel cell hybrid bus (FCHB) was proposed. Research indicates that determining an appropriate start time through deep reinforcement learning algorithms can minimize idle time and energy consumption in fuel cell buses due to frequent start/stop cycles at constant velocities [23,24]. The Pontryagin minimum principle (PMP) was employed to establish both velocity profiles and power split trajectories that minimized total energy consumption along designated routes in [25]. A co-optimization method grounded in PMP was suggested for speed planning and energy management of FCVs [26]. Additionally, a bi-level convex optimization framework for eco-driving FCVs was developed to navigate multiple signalized intersections [27]. The co-optimization of energy management and eco-driving was proposed for FCVs via improved hierarchical MPC [28]. Furthermore, a multi-performance enhanced eco-driving strategy utilizing the stein soft actor-3-critic algorithm was introduced for connected FCHBs [29]. A hierarchical EMS was proposed for FCHBs considering traffic information near the bus stops [30]. A hierarchical intelligent energy-saving control strategy tailored to predict traffic flow dynamics was proposed for FCHBs [31].

In summary, numerous methods have been developed for eco-driving strategies at intersections, achieving remarkable improvements in mobility fuel economy and real-time applicability. Many of the strategies have been implemented on EVs, HEVs, and FCVs. However, urban public transport systems utilizing FCHBs inevitably encounter challenges due to frequent station stops, extended idling periods, and traffic light constraints. Consequently, the development of an energy-saving velocity planning strategy (EVPS) and EMS approaches has proven to be effective in reducing idle time, start/stop durations, and overall energy consumption.

This paper adopts a practical approach to investigate the energy-saving potential of a demonstration FCHB operating within a real urban road environment. A cooperative eco-driving control method is proposed that integrates EVPS with Q-learning-based EMS. This methodology addresses the practical challenges associated with velocity planning and energy management by segmenting them into two distinct sub-problems. The proposed approach not only facilitates multi-objective optimization but also alleviates pressure on the controller. The EVPS component concentrates on velocity planning at multi-signalized intersections and bus stations, while the Q-learning-based EMS component focuses on power distribution. This comprehensive strategy aims to tackle real-world issues such as excessive idle time, high energy consumption costs, and limited operational lifespan of the FCS for FCHBs. This paper presents two significant contributions toward addressing the challenges faced by eco-driving in FCHB.

First, an online EVPS tailored specifically for FCHBs is introduced, utilizing data from three demonstration routes and an eco-driving velocity from DP-based EMS. The proposed EVPS incorporates signal phase and time (SPAT) information along with precise location of bus stations, an essential factor often overlooked in traditional eco-driving strategies. Compared to real-based driving and MIDM-based VPS, EVPS exhibits significant advantages with respect to time savings, stopping duration, time savings rate, and overall pass efficiency.

Second, a collaborative optimization method named EVPS-based EMS is proposed, which integrates the EVPS with a Q-learning-based EMS to enhance eco-driving for FCHBs. The results indicate that the proposed EVPS-based EMS achieves a remarkable reduction in equivalent hydrogen consumption per 100 km by over 21.35%.

The remainder of this paper is structured as follows. Section 2 introduces the FCHB's architecture and driving route. The EVPS and the Q-learning-based EMS are proposed in Section 2 and Section 3, respectively. The validity of cooperative velocity planning and EMS for FCHB is verified in Section 4. Finally, the main conclusions of the study are discussed in Section 5.

2. The FCHB structure and driving route

2.1. Parameter and structure of FCHB

The powertrain structure and the main parameters of the demonstration FCHB are shown in Fig. 1 and Table 1. The FCHB propulsion system consists of several key components, including an electric motor, an FCS, a battery pack, a DC/DC converter, and a high voltage distribution unit (PDU). The vehicle control unit coordinates various control units, such as motor control unit (MCU), fuel cell control unit (FCCU), and battery management system (BMS). The power balance of the FCHB can be expressed as follows,

$$P_{\mathrm{dem}} = P_{\mathrm{f}}\eta_{\mathrm{dc}} + P_{\mathrm{b}} \tag{1}$$

where

$$P_{\mathrm{dem}} = \frac{v_{\mathrm{a}}(mgf + \frac{C_{\mathrm{D}}Av_{\mathrm{a}}^2}{21.15} + \delta m\frac{\mathrm{d}v_{\mathrm{a}}}{\mathrm{d}t})}{\eta_{\mathrm{t}}\eta_{\mathrm{m}}} + P_{\mathrm{aux}} \tag{2}$$

P_{f} and P_{b} are the output power of the FCS and the battery pack, respectively. η_{dc} is the efficiency of the DC/DC converter. m represents the vehicle mass, g is the gravity acceleration. f and C_{D} are the rolling resistance and drag coefficients, respectively. A is the frontal area of the FCHB, and δ is the conversion coefficient of the rotating mass. η_{t} and η_{m} are the mechanical transmission efficiency and the motor efficiency, respectively.

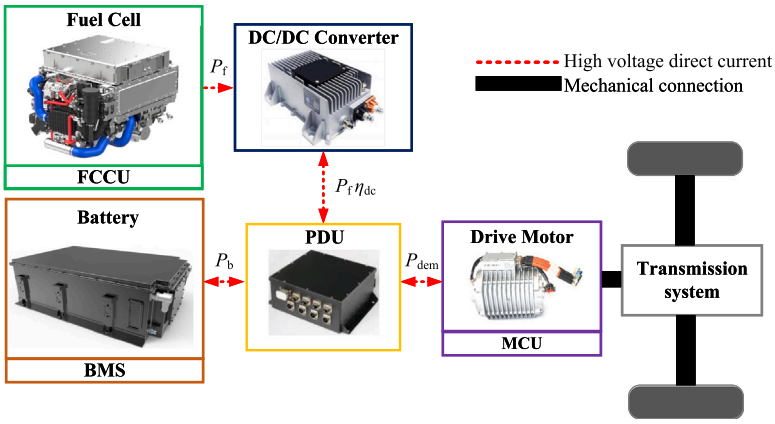

Fig. 1. The structure of the FCHB powertrain system.

Table 1
Main parameters.

Items	Parameters	Value
FCHB	Mass (kg)	14 350
	Frontal area (m^2)	7.13
	Mechanical transmission efficiency	0.95
	DC/DC efficiency	0.99
Motor	Max power (kW)	200
Fuel cell	Rate power (kW)	47
	Number of cells	140
Battery	Rate capacity (Ah)	173
	Cell rated voltage (V)	3.22
	Number of cells	162

2.2. FCHB actual driving route analysis

The demonstration data for three routes of the FCHB are collected to optimize the driving velocity. The operational routes of the FCHB demonstration, namely Route i (where i = 1 to 3), are situated in Chengdu, China, as illustrated in Fig. 2. Route 1 comprises 8 traffic lights ($L1_j$, where j = 1 to 8) and 10 bus stations ($S1_k$, where k = 1 to 10). Route 2 features 18 traffic lights ($L2_j$, where j = 1 to 18) and 17 bus stations ($S2_k$, where k = 1 to 17). Route 3 includes 10 traffic lights ($L3_j$, where j = 1 to 10) and 5 bus stations ($S3_k$, where k = 1 to 5). Herein $L1_j$ and $S1_k$ denote the locations of the jth traffic light and the kth bus station for Route 1, respectively. Similarly, $L2_j$ and $S2_k$ are defined for Route 2, $L3_j$ and $S3_k$ are defined for Route 3. For all three routes, Table 2 presents the distances from each bus station Si_k to the first bus station Si_1. The total lengths of Routes 1, 2, and 3 are 11.574 km, 11.039 km, and 9.840 km, respectively. Notably, both the density of traffic lights and distribution of bus stations on Route 2 exceed those observed on Route 1 at over a comparable distance.

Furthermore, these three routes can be classified into distinct categories based on geographic location and roadway characteristics: Suburban (Route 1), Urban + Suburban (Route 2), and Urban (Route 3). The signal phases along with timing details for each route's traffic lights are summarized in Table 3, which includes accumulated distance (D) from each respective traffic light to the first bus station, and periods (T) associated with each traffic light cycle. Periods (T) comprises red light duration (T_R) and green light duration (T_G), such that $T = T_R + T_G$. It is important to note that yellow light durations have not been overlooked. Instead, they have been incorporated into red light time in an effort to enhance driving safety during operations [32].

Three representative demonstration operation trajectories are illustrated in Fig. 3. In actual operations, the overall velocity of Route 1 surpasses that of Route 2 and Route 3, with a maximum velocity v_{max} reaching 53 km/h. The average velocity ranges from 20 km/h to 26 km/h, while the average driving velocity (excluding instances when the vehicle is stationary) falls between 31 km/h and 33 km/h. In Fig. 3-(a), the total travel time for Route 1 is recorded at 1714 s, and during which the FCHB made six stops at traffic lights, excluding $L1_1$ and $L1_2$. Between $L1_3$ and $L1_8$, idle times at intersections are measured as follows: 44 s, 88 s, 16 s, 15 s, 42 s, and 8 s, respectively. The cumulative idle time across these stops totals to a duration of 213 s. Consequently, the passage rate at signalized intersections stands at a mere 25.00%. In Fig. 3-(b), it is noted that the total travel time for Route 2 amounts to 1900 s, with 8 stops encountered due to traffic lights. The cumulative idle time during these stops reaches 493 s, distributed as follows: 24 s, 40 s, 94 s, 30 s, 73 s, 40 s, 75 s, 117 s. Thus yielding the passage rate is 55.56% at signalized intersections. Fig. 3-(c) presents data indicating that on Route 3, the FCHB experienced a travel duration of 1575 s, encountering red lights 6 times at locations $L3_1$, $L3_4$, $L3_5$, $L3_6$, $L3_9$, and $L3_{10}$. Stopping durations observed at these signalized intersections are 7 s, 18 s, 42 s, 41 s, 76 s, and 125 s, respectively. This results in a cumulative stopping time totaling 309 s, alongside a passing efficiency of 40.00%. Specific Real-based driving data can be found in Table 4.

It is noteworthy that Real-based driving experiences involve numerous frequent stops coupled with prolonged idle periods. These factors contribute significantly to diminished comfort levels, increased hydrogen consumption rates, reduced FCS lifespan, and elevated operational costs.

3. EVPS

This subsection proposes an EVPS grounded in the actual signal information and real vehicle status aimed at reducing accumulated idle time, enhancing passage rates at signalized intersections, and promoting eco-driving practices. For simplicity, this study focuses exclusively on a single FCHB operating within a designated bus lane while excluding considerations related to road queuing phenomena, external factors, and other vehicles.

3.1. Parameters setting for EVPS

To formulate the EVPS, several parameters are established in advance, including maximum acceleration a_{max}, minimum deceleration a_{min}, maximum velocity v_{max}, minimum velocity v_{min}, and eco-driving velocity v_{eco}. Based on analysis of 316,141 pieces of real driving data from FCHB collected over a period of 10 days, the values for a_{max} and a_{min} are set to ± 1.5 m/s^2. For computational convenience, this study also establishes a minimum velocity limit v_{lim} of 1.5 km/h. The distance for velocity planning d_y is determined based on the range of dedicated short range communication (DSRC), which is set as 200 m [33].

A DP-based EMS is employed to calculate the equivalent hydrogen consumption per 100 km under constant velocity conditions to facilitate the identification of the optimal v_{eco}. Fig. 4 illustrates the relationship

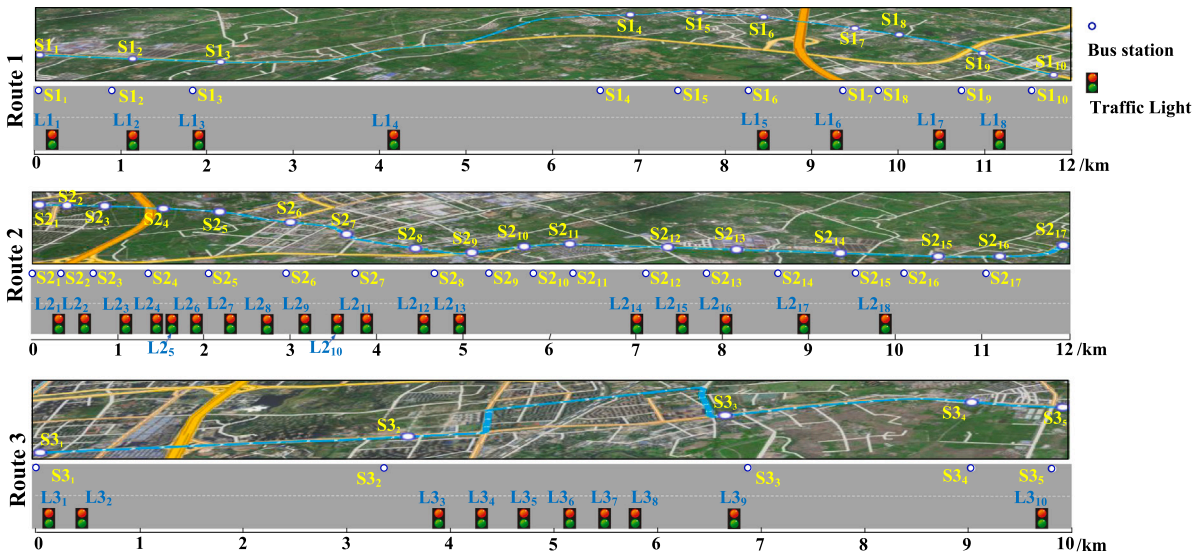

Fig. 2. The Route 1, Route 2 and Route 3 of the demonstration driving routes of FCHB in Chengdu, China. Li_j represents the jth traffic light on the ith route, while Si_k represents the kth bus station on the ith route, where i = 1, 2, 3, j = 1, …, 18, and k = 1, …,17. For example, $L1_1$ is the first traffic light on the Route 1, and $S2_1$ corresponds to the first bus station on the Route 2.

Table 2
The distance from the bus station Si_k to the first bus station Si_1.

Route 1	Si_k	$S1_1$	$S1_2$	$S1_3$	$S1_4$	$S1_5$	$S1_6$	$S1_7$	$S1_8$	$S1_9$	$S1_{10}$
	distance/m	0	945	1827	6544	7465	8272	9294	9777	10 753	**11 574**
Route 2	Si_k	$S2_1$	$S2_2$	$S2_3$	$S2_4$	$S2_5$	$S2_6$	$S2_7$	$S2_8$	$S2_9$	$S2_{10}$
	distance/m	0	311	724	1370	2056	2976	3772	4667	5274	5786
	Si_k	$S2_{10}$	$S2_{11}$	$S2_{12}$	$S2_{13}$	$S2_{14}$	$S2_{15}$	$S2_{16}$	$S2_{17}$		
	distance/m	5786	6255	7156	7788	8705	9570	10 106	**11 039**		
Route 3	Si_k	$S3_1$	$S3_2$	$S3_3$	$S3_4$	$S3_5$					
	distance/m	0	3283	6909	9054	**9840**					

Table 3
The signal phase and time of traffic lights for three routes.

Route	Li_j	D /m	T /s	T_R /s	T_G /s	Li_j	D /m	T /s	T_R /s	T_G /s
1	$L1_1$	180	135	31	104	$L1_5$	8391	112	34	78
	$L1_2$	1165	160	60	100	$L1_6$	9231	98	36	62
	$L1_3$	1862	120	50	70	$L1_7$	10 498	110	65	45
	$L1_4$	4146	132	98	34	$L1_8$	11 185	74	34	40
2	$L2_1$	294	116	63	53	$L2_{10}$	3575	72	39	33
	$L2_2$	574	118	35	83	$L2_{11}$	3842	182	121	61
	$L2_3$	1033	114	31	83	$L2_{12}$	4528	84	42	42
	$L2_4$	1405	113	29	84	$L2_{13}$	4937	125	88	37
	$L2_5$	1613	139	26	113	$L2_{14}$	7000	260	140	120
	$L2_6$	1934	119	55	64	$L2_{15}$	7593	140	38	102
	$L2_7$	2271	113	63	50	$L2_{16}$	8047	136	30	106
	$L2_8$	2720	182	137	45	$L2_{17}$	8926	215	128	87
	$L2_9$	3374	102	49	53	$L2_{18}$	9892	168	81	87
3	$L3_1$	87	87	42	45	$L3_6$	5096	90	50	40
	$L3_2$	392	98	53	45	$L3_7$	5486	76	36	40
	$L3_3$	3808	140	90	50	$L3_8$	5704	105	45	60
	$L3_4$	4181	130	45	85	$L3_9$	6717	166	82	84
	$L3_5$	4637	140	60	80	$L3_{10}$	9724	205	184	21

Note: D is accumulated distance from Li_j to Si_1.
T is the period of the traffic light.
T_R and T_G are the duration of red light and green light, respectively.
Li_j is the jth traffic light on the ith route.

between the static equivalent hydrogen consumption per 100 km corresponding to constant velocities ranging from 1 km/h to 53 km/h. It should be noted that equivalent hydrogen consumption per 100 km remains relatively low for velocities ranging from 20 km/h to 35 km/h, with minimal consumption observed at approximately 28 km/h.

Taking into account Real-based travel data, the energy-saving driving velocity v_{eco} has been established at approximately 32.58 km/h. Consequently, essential parameters assumed for FCHB are summarized in Table 5.

3.2. EVPS frame

In accordance with characteristics outlined in Section 2.2 regarding FCHB routes, areas designated for velocity planning are categorized into bus stations and signalized intersections. For the bus station, when the FCHB detects a stop located 200 m ahead, it will initiate gradual deceleration to ensure smooth arrival at said stop while maintaining a driving distance within planned speed parameters equivalent to d_y. Consequently, the VPS specifically tailored for the bus station can be expressed as

$$v = \sqrt{2d_y a_{de} + v_0^2} \tag{3}$$

For signalized intersections, prior consideration must be given to SPAT information along with any remaining durations of both red and green lights. Furthermore, to promptly revert back to an energy-saving velocity v_{eco} without prolonging transit times unnecessarily during recovery phases of acceleration or deceleration maneuvers, no adjustment distances shall apply within these sections. Thus, the traffic signals can be predominantly categorized into two phases: green light phase and red light phase.

3.2.1. Green light phase

Three distinct scenarios are identified predicated upon expected residual durations of green light time t_g, including long time left, short time left, and very short time left. A detailed schematic representation

Table 4
Data of the three routes traveling at intersections.

Route	Traveling time (s)	Number of stop	Stop time (s)	Total stop time (s)
1	1714	6	44/88/16/15/42/8	213
2	1900	8	24/40/94/30/73/40/75/117	493
3	1575	6	7/18/42/41/76/125	309

Number of stop: the total number of stop when the vehicle encounters a red light.
Stop time: the stop time when the vehicle encounters a red light.
Total stop time: the sum of stop times.

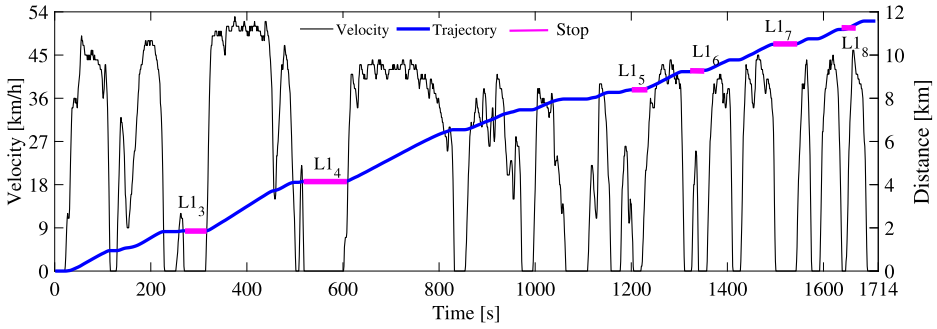

(a) The Route 1.

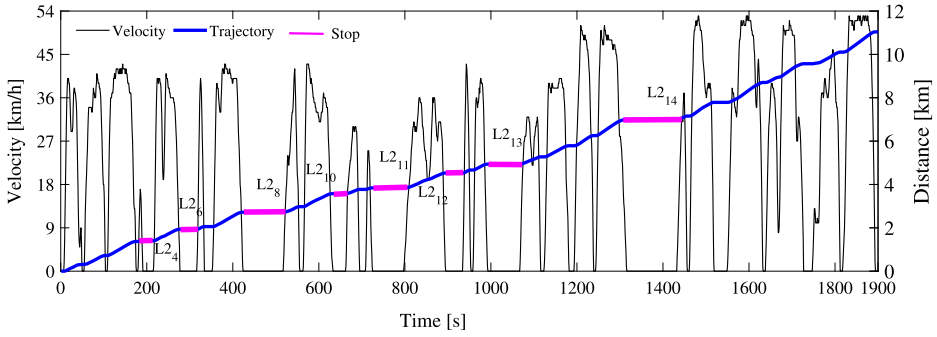

(b) The Route 2.

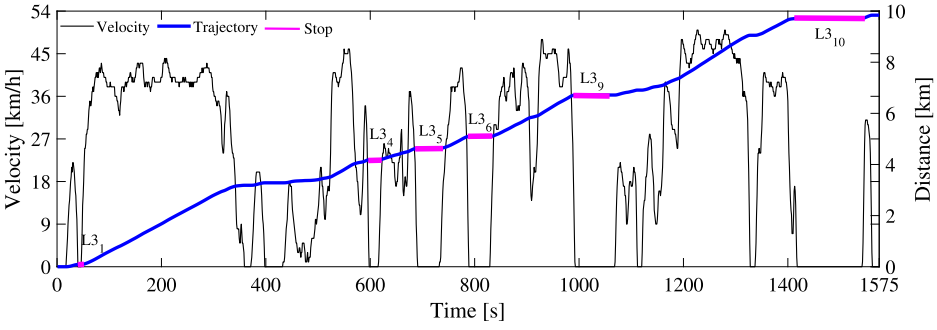

(c) The Route 3.

Fig. 3. Demonstration velocity and trajectory of FCHB in Chengdu, China.

illustrating vehicle trajectories across these three pre-green-light-phase conditions is depicted in Fig. 5-(a).

Scene 1: Long time left. The long time left scene's determining equation can be expressed as follows,

$$t_g \geq \frac{d_y}{v_0} \tag{4}$$

In Scene 1's EVPS, if $v_0 < v_{eco}$, the FCHB will accelerate the speed with a_{max} in t s to v_{eco} and pass the signalized intersection with constant velocity (v_{eco}). For alternative instances, the FCHB will through the signal intersection with the initial velocity v_0. The FCHB seamlessly navigates past such intersections adopting what we term 'constant-velocity passage' methodology which may further be encapsulated mathematically below,

$$v = \begin{cases} v_0 + a_{max}t \text{ to } v_{eco}, & v_0 < v_{eco} \\ v_0, \text{ others} \end{cases} \tag{5}$$

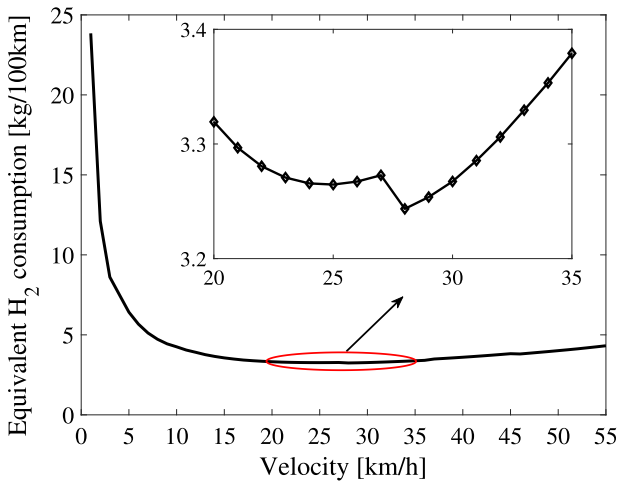

Fig. 4. Relationship between equivalent hydrogen consumption per 100 km and velocity.

Table 5
Assumptions of basic FCHB.

Basic parameters	Description
Maximum velocity	v_{max} = 53 km/h
Minimum velocity	v_{min} = 0 km/h
Minimum velocity limit	v_{lim} = 1.5 km/h
Maximum acceleration	a_{max} = 1.5 m/s^2
Minimum deceleration	a_{min} = −1.5 m/s^2
Velocity planning distance	d_y = 200 m
Remain of green light time	t_g
Remain of red light time	t_r
Eco-driving velocity	v_{eco} = 32.58 km/h

Scene 2: Short time left. The short time left scene's determining equation can be expressed as follows,

$$\frac{d_y - \frac{v_{max}^2 - v_0^2}{2a_{max}}}{v_{max}} + \frac{v_{max} - v_0}{a_{max}} < t_g < \frac{d_y}{v_0} \tag{6}$$

In scene 2, the EVPS is formulated as follows. When $v_0 < v_{eco}$, and the time (where the FCHB accelerates with maximum acceleration a_{max} to v_{eco} and then travels at a constant velocity to reach the signalized intersection) is less than t_g, the FCHB can accelerate to v_{eco} and then travel at a constant velocity (v_{eco}). Othercases, the FCHB is controlled to accelerate with a_{max} until it reaches v_{max} and pass the signal intersection. In this scene, FCHBs are able to pass the signal after accelerating. Thus, an acceleration strategy is employed. The mathematical expression for the velocity trajectory under this strategy is provided as follows,

$$v = \begin{cases} v_0 + a_{max}t \text{ to } v_{eco}, v_0 < v_{eco} \text{ and } t_g > \frac{d_y - \frac{v_{eco}^2 - v_0^2}{2a_{max}}}{v_{eco}} + \frac{v_{eco} - v_0}{a_{max}} \\ v_0 + a_{max}t \text{ to } v_{max}, \text{ others} \end{cases} \tag{7}$$

Scene 3: Very short time left. The very short time left scene's determining equation can be expressed as follows

$$0 < t_g < \frac{d_y - \frac{v_{max}^2 - v_0^2}{2a_{max}}}{v_{max}} + \frac{v_{max} - v_0}{a_{max}} \tag{8}$$

In this scene, the FCHB accelerates to the maximum velocity v_{max} starting from v_0, yet still cannot pass through, it must resort to a deceleration and stop strategy. The mathematical expression of the velocity trajectory is outlined as follows,

$$v = v_0 + \frac{-v_0^2}{2d_y}t \text{ to } 0 \tag{9}$$

3.2.2. Red light phase

Similarly, three distinct scenes, including very long time left, long time left, and very short time left, are identified based on the anticipated remaining time of the red light t_r. A specific simulated schematic diagram illustrating driving trajectories for these three scenes preceding the red light phase is illustrated in Fig. 5-(b).

Scene 4: Very long time left. The very long time left scene's determining equation can be expressed as follows,

$$t_r > \frac{d_y - \frac{v_{lim}^2 - v_0^2}{2a_{min}}}{v_{lim}} + \frac{v_{lim} - v_0}{a_{min}} \tag{10}$$

The mathematical expression for vehicle velocity under this strategy is as follows,

$$v = v_0 + \frac{-v_0^2}{2d_y}t \tag{11}$$

Scene 5: Long time left. The long time left scene's determining equation can be expressed as follows

$$\frac{d_y}{v_0} < t_r < \frac{d_y - \frac{v_{lim}^2 - v_0^2}{2a_{min}}}{v_{lim}} + \frac{v_{lim} - v_0}{a_{min}} \tag{12}$$

In Scene 5, the EVPS is formulated as follows. If $v_{eco} < v_0 < v_{max}$, one must assess whether sufficient time exists to travel to the intersection at a constant velocity after decelerating to v_{eco} at v_0. And the required time exceeds t_r, the FCHB should first decelerate and then pass through the intersection at a constant velocity at v_{eco}. Under other conditions, the FCHB will decelerate until reaching the intersection with v_0 traveling t_r time. In Scene 5, the vehicles successfully navigate past the signalized intersection following deceleration. Hence, a deceleration passing strategy is adopted. The mathematical expression for vehicle velocity under this strategy is as follows,

$$v = \begin{cases} v_0 + a_{min}t \text{ to } v_{eco}, v_{eco} < v_0 < v_{max} \text{ and } t_r < \frac{d_y - \frac{v_{eco}^2 - v_0^2}{2a_{min}}}{v_{eco}} + \frac{v_{eco} - v_0}{a_{min}} \\ v_0 - \frac{2(d_y - v_0 t_r)}{{t_r}^2}t, \text{ others} \end{cases} \tag{13}$$

Scene 6: Very short time left. The very short time left scene's determining equation can be expressed as follows

$$0 < t_r \le \frac{d_y}{v_0} \tag{14}$$

In Scene 6, the EVPS is formulated as follows. If $v_0 \le v_{eco}$, the FCHB is controlled to maintain a constant velocity of v_0 to reach the signalized intersection. In other cases, the FCHB is instructed to decelerate to v_{eco} and proceed through the intersection. In scene 6, the FCHB can traverse the signalized intersection at a constant velocity. Thus, a constant velocity strategy is employed. The mathematical representation of the vehicle's velocity trajectory under this strategy is as follows,

$$v = \begin{cases} v_0, v_0 \le v_{eco} \\ v_0 + a_{min}t \text{ to } v_{eco}, \text{ others} \end{cases} \tag{15}$$

In summary, there are six distinct passing scenes at signalized intersections, each corresponding to one of six passing decision strategies: (1) Green light constant velocity strategy. (2) Green light acceleration strategy. (3) Green light slow down and stop strategy. (4) Red light slow down and stop strategy. (5) Red light decelerate strategy. (6) Red light constant velocity strategy.

Considering both the states of the FCHB and its interaction with vehicles and road infrastructure, an overview of EVPS flow at signalized intersections is illustrated in Fig. 6.

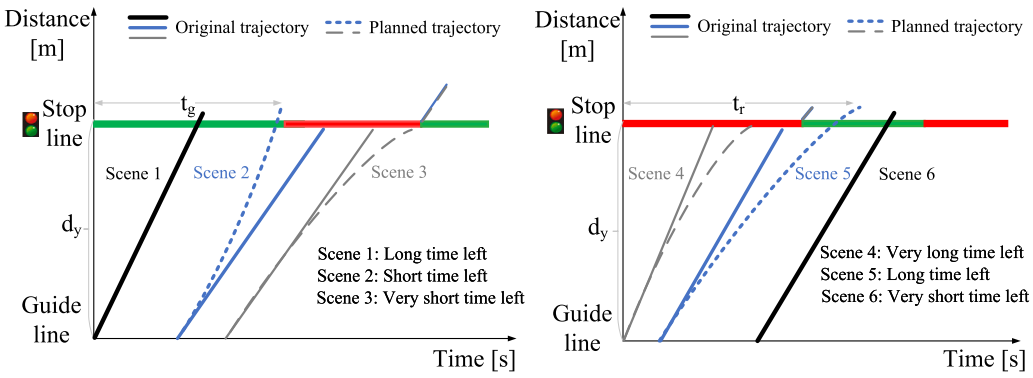

Fig. 5. The trajectory of traffic light.

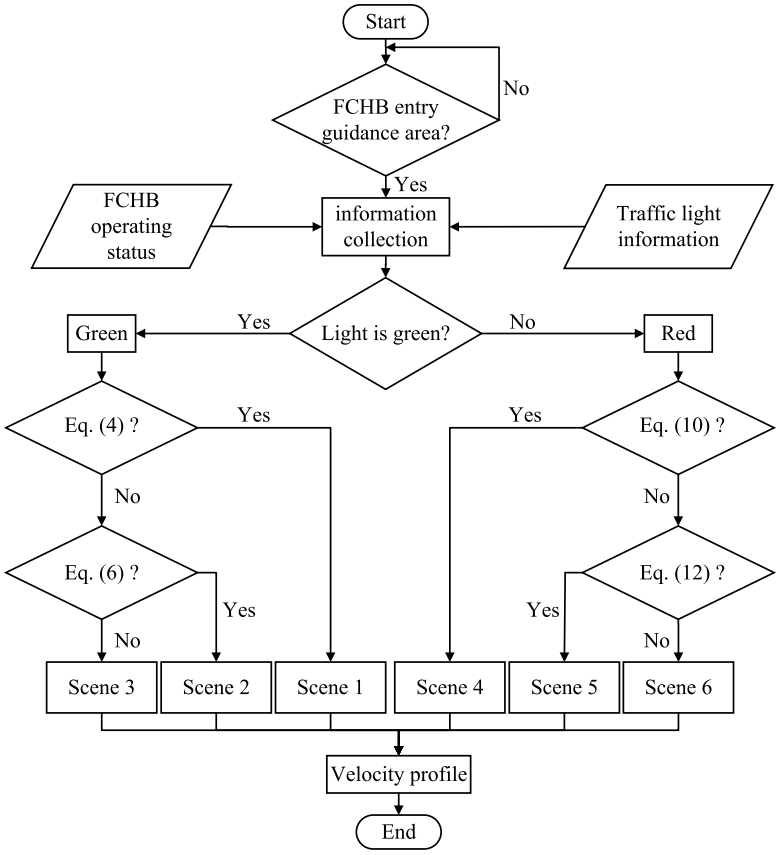

Fig. 6. EVPS at signalized intersection.

4. Q-learning-based EMS

To facilitate effective velocity planning for the FCHB, an EMS based on a model-free Q-learning algorithm is implemented. The Q-learning algorithm represents a robust framework within artificial intelligence and control theory that comprises five fundamental components: agent, state, action, environment, and reward function [34]. Herein, EMS serves as the agent while states are defined by discrete SOC levels along with demand power (P_{dem}) for the FCHB. The variable P_f represents discrete actions variable. r_s^a is the reward the agent receives with action.

The primary objective of this algorithm is to maximize cumulative state–action Q-values, which necessitates establishing a Q-table for storing the Q-value alongside defining an appropriate reward function. It constantly updates the Q-table by repeating every iteration number N ($N = 1, 2, 3...$) and state j ($j = 1, 2, 3...$), allowing adaptive and optimal strategy selection. The ultimate goal is to develop an optimal EMS that minimizes energy consumption and prolongs the FCS's lifetime. The Q-learning-based EMS seeks to maximize the cumulative return of state–action pairs, represented by the optimization objective function $Q^*(s, a)$, which can be expressed as follows,

$$Q^*(s,a) = r_s^a + \gamma \sum_{s'} P_{s,s'} \max_{a'} Q^*(s', a') \tag{16}$$

where s' and a' are the state and action variables at the next moment, respectively. s and a are the state and action variables at the current moment, respectively. γ denotes the discount rate. $P_{s,s'}$ represents the state transfer probability of P_{dem}.

The reward function r_s^a is the immediate reward obtained after taking action a in the current state s. It consists of four main components: the sum of the hydrogen consumption of the FCS and the equivalent

hydrogen consumption of the battery, the maintenance of the battery SOC, and changes in power and decay of the FCS [15]. r_s^a is expressed as follows,

$$r_s^a = -(\omega_1 r(g_{h_2}) + \omega_2 r(|soc - soc_{ref}|^2) + \omega_3 r(|P_{f,t} - P_{f,t-1}|) + \omega_4 r(FC_{dr})) \tag{17}$$

where the values of the weight parameters ω_1, ω_2, ω_3, and ω_4 are determined after numerous experiments. The hydrogen economy function $r(g_{h_2})$ is the sum of the FCS's instantaneous hydrogen consumption and the battery's equivalent hydrogen consumption. It is expressed as follows [35],

$$r(g_{h_2}) = \frac{1000 P_f}{LHV_{h_2}\eta_{fc}} + \begin{cases} \frac{P_b}{\eta_{di}\eta_{ch}} \frac{C_{fav}}{P_{dcav}}, P_b \geq 0 \\ P_b \eta_{ch}\eta_{di} \frac{C_{fav}}{P_{dcav}}, \text{others} \end{cases} \tag{18}$$

where LHV_{h_2} represents the low calorific value of hydrogen, equal to 1.2×10^8 J/kg. η_{fc} is the efficiency of the FCS. η_{ch} and η_{di} represent the battery's charge and discharge efficiency, respectively. $\overline{\eta_{ch}}$ and $\overline{\eta_{di}}$ represent the battery's average charge and discharge efficiency, respectively. C_{fav} is the average instantaneous hydrogen consumption of the FCS. P_{dcav} denotes the average power of the DC/DC converter.

The battery SOC maintenance function is expressed as $r(|soc - soc_{ref}|^2)$. soc and soc_{ref} represent the actual and reference values of the battery SOC, respectively. The FCS power fluctuation function is expressed as $r(|P_{f,t} - P_{f,t-1}|)$. $P_{f,t}$ and $P_{f,t-1}$ are the FCS power at the current moment and the previous moment, respectively.

The FCS decay function $r(FC_{dr})$ is expressed as

$$r(FC_{dr}) = \frac{1}{1 + e^{-FC_{dr}}} \tag{19}$$

where the corresponding aging degradation FC_{dr} is presented as follows [35]:

$$FC_{dr} = K_p\left(\left(k_1 t_1 + k_2 n_1 + k_3 n_2 + k_4 t_2\right) + \varphi\right) \tag{20}$$

where FC_{dr} represents the degradation of FCS. K_p is a correction coefficient used to account for differences between the experimental and real environments. k_1, k_2, k_3, and k_4 denote the degradation factors for idle, start-stop, variable load, and heavy load conditions, respectively. t_1, t_2, n_1, and n_2 represent the duration and frequency of the four operating cycles (idle, start-stop, variable load, and heavy load) for FCS, respectively. φ denotes the natural degradation rate of the FCS over time. The specific values for these parameters can be found in Ref. [35].

The flow of the Q-learning algorithm implemented in FCHB EMS is shown in Fig. 7, where S and A represent collections of the state and action variables, respectively.

5. Simulation and validation

The core concept of the EVPS-based EMS is illustrated in Fig. 8, which encompasses a collaborative control framework. Initially, focusing on essential parking scenes such as signalized intersections and bus stations present on actual roadways, the EVPS is employed to plan velocity for the FCHB. Subsequently, utilizing the velocity command generated by the EVPS, the Q-learning-based EMS is activated to manage power distribution across the battery pack and the FCS.

5.1. The effectiveness of EVPS

In this subsection, simulation experiments are conducted along three routes to achieve an improved velocity profile and validate the adaptability of the EVPS. A modified intelligent driver model (MIDM) [9] serves as a benchmark for comparisons purposes. To more clearly assess the passing ability of the proposed strategy at signalized intersections, we ensure that parking times at bus stations under Real-based driving, MIDM-based VPS, and EVPS are consistent.

Table 6
Route1: Results for three VPSs.

VPS	Travel time/s	Saving time/s	Idling time/s	Total idle time/s	Saving idle time rate	Passing efficiency
Real	1714	–	44/88/16/15/42/8	213	–	25.00%
MIDM	1667	47	6/12	18	91.55%	75.00%
EVPS	1672	42	9	9	95.77%	87.50%

Saving idle time rate: The saving rate of the total idle time compared to Real-based driving methods.
Passing efficiency: The ratio of the number of FCHB passes to the number of intersections.

5.1.1. Route 1

Trajectories from both VPS approaches on Route 1 are illustrated in Fig. 9. The results indicate that performance using EVPS outperforms MIDM in terms of reducing both stop frequency and access delays. The velocity trajectory corresponding to MIDM is depicted in Fig. 9-(a). When approaching $S1_3$ with $L1_3$ ahead displaying a red light signal, smooth passage becomes impossible. Consequently, two instances requiring deceleration occur, first at $L1_3$ followed by another at $L1_4$. Conversely, Fig. 9-(b) presents data from the EVPS approach where only one stop occurs at intersections with a total stopping duration of just 9 s for FCHB operations. The FCHB passes most sections adhering to eco-driving speed (v_{eco}), and maintains efficient movement. However, due to the proximity between $L1_3$ and $S1_3$, locations requiring gradual acceleration after a brief stop occur following a halt at $S1_3$. The signal $L1_3$ ahead is in the red phase, with an extended remaining time. Consequently, the FCHB adopts the strategy of deceleration and stopping while waiting the commencement of the next green phase.

The space–time results of the three strategies are summarized in Fig. 9-(c), where the green line segment represents the duration of the green light. Due to varying controllability among these strategies, the time windows during which the FCHB passes traverses signalized intersections differ significantly. As illustrated by the black dotted line and purple dot line, Real-based driving and MIDM-based VPS demonstrate high acceleration prior to reaching the 4th light, resulting in a stop at that intersection. In contrast, EVPS is more adept at planning velocity with fewer instances of starting/stopping and reduces idling time.

Table 6 presents detailed outcomes for all three proposed VPSs. The idling times under both MIDM-based and EVPS-based methods are markedly lower compared to those observed with Real-based driving method, 18 s and 9 s, respectively. Although overall driving time is reduced by 5 s using MIDM-based VPS, it is noteworthy that EVPS substantially decreases idling time at signalized intersections. The idle time saving rate associated with EVPS improved by 4.22%, while passing efficiency increased by 12.50% relative to the MIDM-based VPS. When compared to Real-based driving methods, EVPS achieved an impressive time saving rate of 95.77% alongside an enhancement in passing efficiency of 87.50%. It is important to emphasize that this proposed EVPS demonstrates superior traffic efficiency at signalized intersections and highlights its effectiveness in promoting eco-driving practices.

5.1.2. Route 2

The trajectories of the two VPSs on Route 2 are illustrates as Fig. 10. On this route, all three strategies enable the FCHB to reach its destination within the expected time frame. The simulation results of vehicle speed planning under the MIDM-based approach are presented in Fig. 10-(a). The vehicle comes to a stop three times at locations $L2_8$, $L2_{11}$ and $L2_{17}$. A red signal is observed from a distance of 100 m before reaching these points. Consequently, the vehicle decelerates and halts. When arriving at each signalized intersection still facing a red lihgt phase, it must wait for the subsequent green phase to commence.

The simulation outcomes based on the EVPS method are depicted in Fig. 10-(b). At location $L2_{17}$, when encountering a red light, this

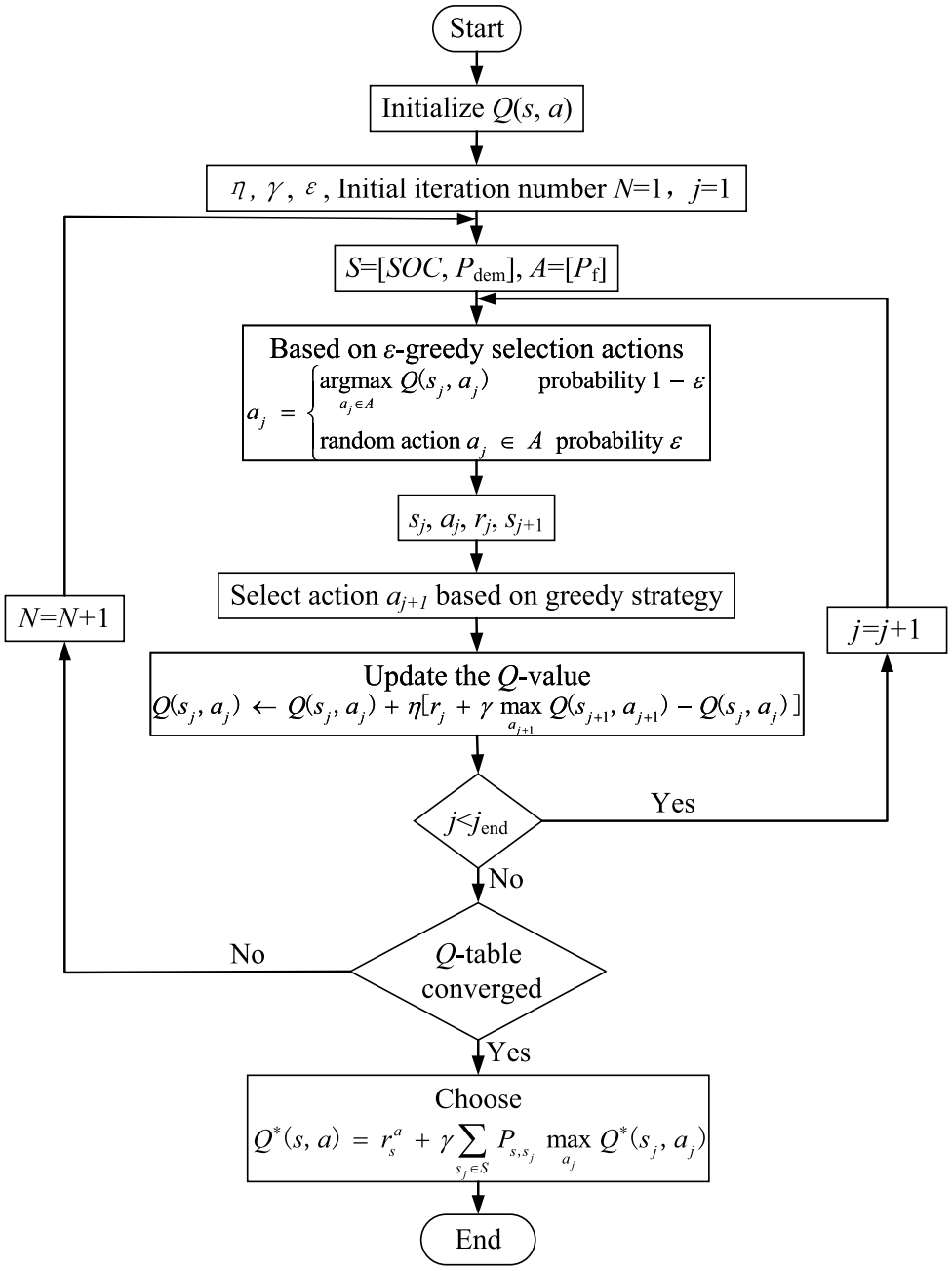

Fig. 7. Flow chart of Q-learning algorithm.

strategy employs a red light deceleration stopping strategy resulting in an idle period of 48 s.

Space–time trajectory diagrams corresponding to all three strategies are presented in Fig. 10-(c). It is evident that while both MIDM-based VPS and EVPS exhibit similar driving trajectories, the proposed EVPS significantly reduces instances of stops due to red lights. For example, when the FCHB passed the 8th light and 11th light, it hit the red light and waited for 94 s and 73 s with the Real-based strategy. It waited for 67 s with the MIDM-based VPS. While the EVPS is capable of successfully passing through the light.

Detailed performance metrics for all three VPSs are summarized in Table 7. Under Real-based driving conditions, total stopping time amounts to an extensive duration of 493 s across 8 stops. It characterizes by prolonged halts including one instance lasting as long as 117 s. Additionally, the total stopping time at the traffic signal is significantly decreased by 151 s and 48 s, resulting in idling time savings of 69.37% and 90.26%, respectively. In terms of intersection passing efficiency, the passing rate for Real-based driving stands at 55.56%, while that for the MIDM-based and EVPS-based methods are 83.33% and 94.44%, representing increases of 27.77% and 38.88% over Real-based driving, respectively. When compared to the MIDM-based VPS, the EVPS-based method demonstrates a idle time saving improvement of 20.89% along with an enhancement in passing efficiency by 11.11%. Notably, the EVPS demonstrates higher passing efficiency compared to the MIDM-based VPS.

5.1.3. Route 3

The vehicle velocity trajectories on Route 3, based on MIDM and EVPS methodologies, are illustrated in Fig. 11. The driving time for vehicles utilizing the MIDM-based approach is recorded at 1382 s, while the total driving time under the EVPS framework is noted as 1379 s. This results in a difference of merely 3 s between the two strategies.

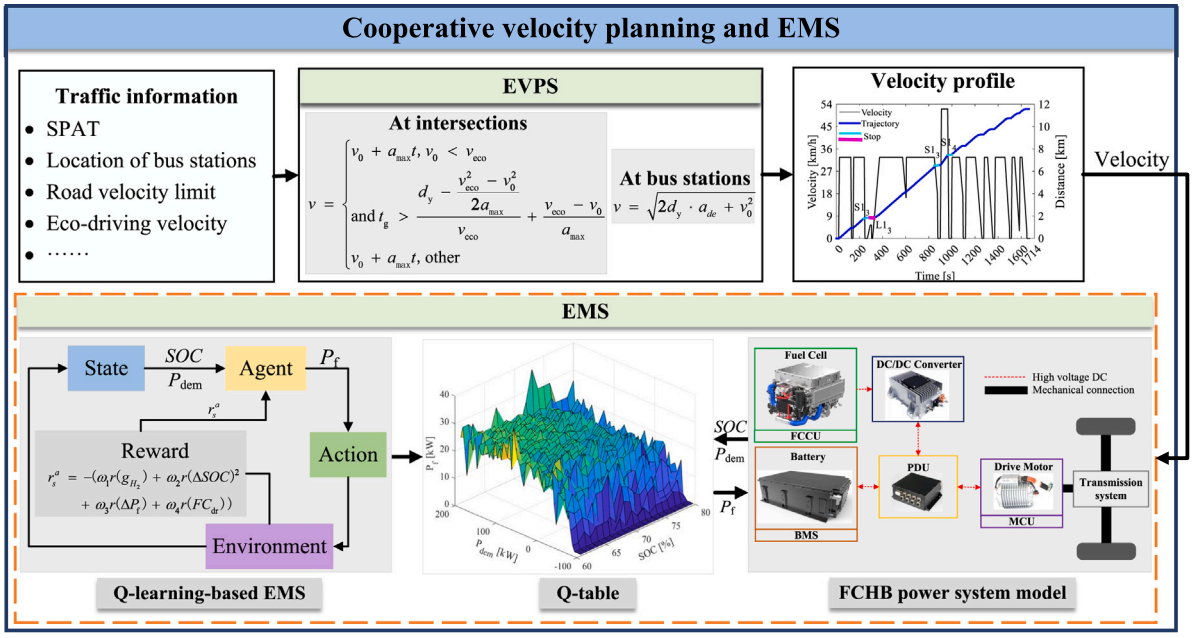

Fig. 8. Framework of the EVPS and Q-learning-based EMS.

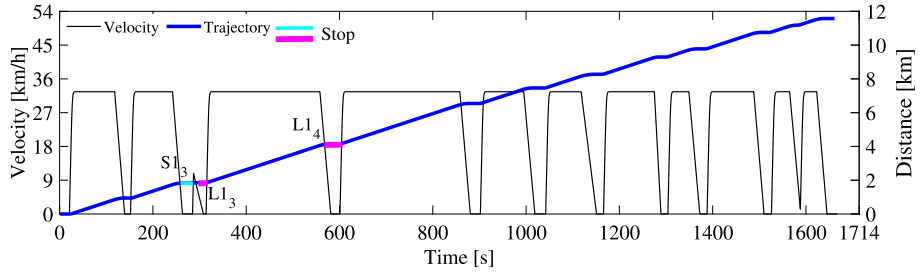

(a) MIDM-based driving

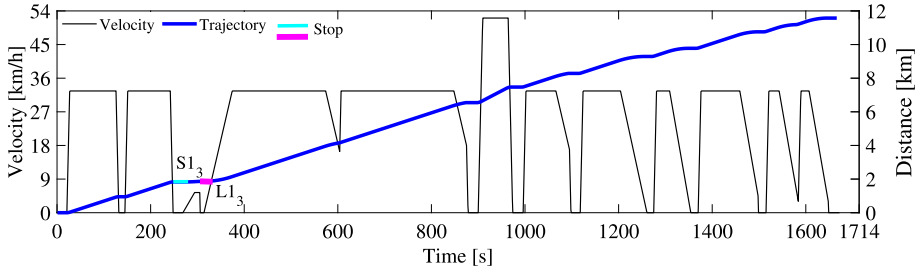

(b) EVPS-based driving

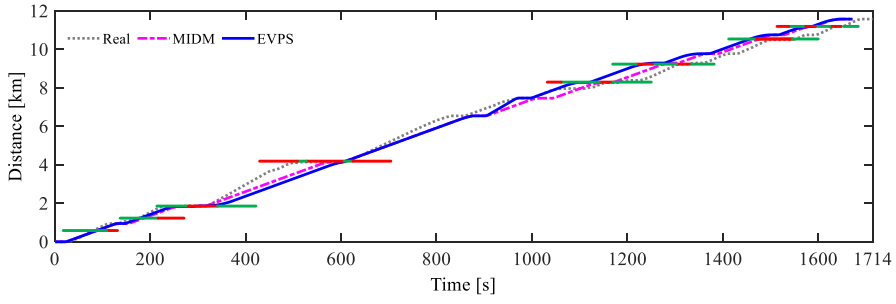

(c) Space-time trajectory for different VPSs

Fig. 9. Route 1: Trajectory of the FCHB.

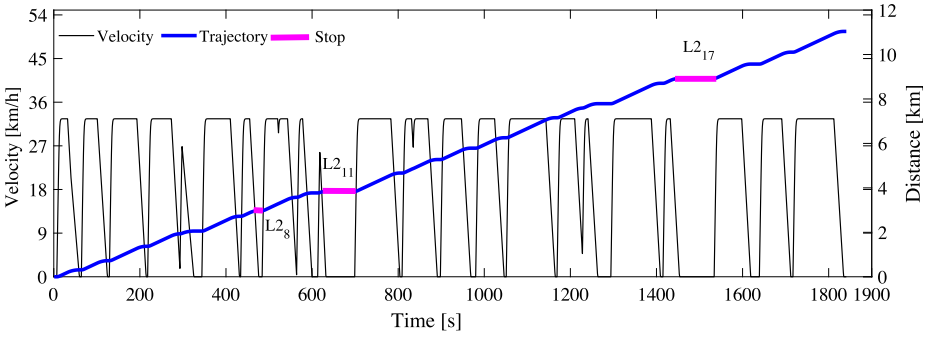

(a) MIDM-based driving

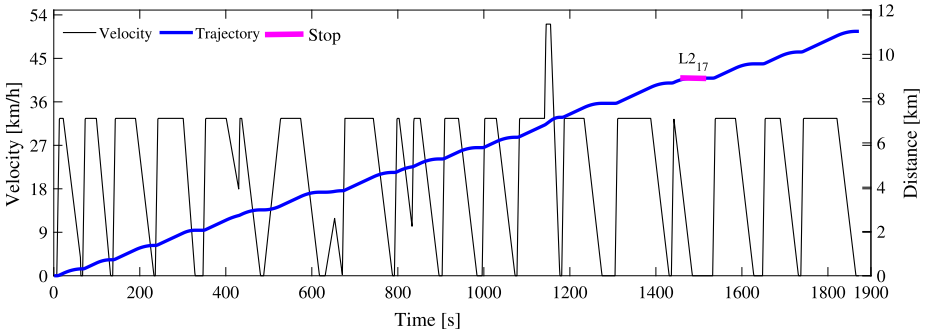

(b) EVPS-based driving

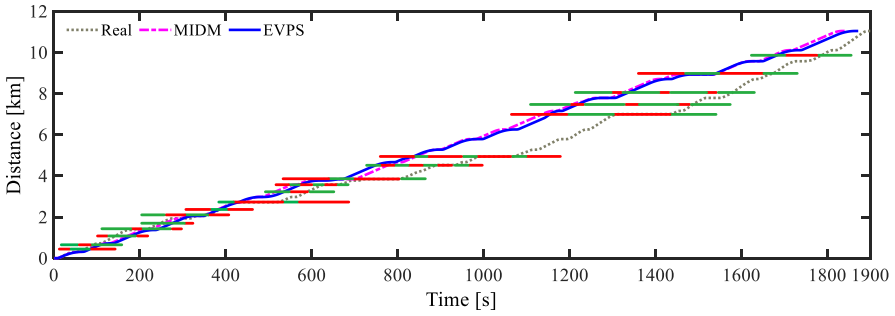

(c) Space-time trajectory for different VPSs

Fig. 10. Route 2: Trajectory of the FCHB.

Table 7
Route2: Results for three VPSs.

VPS	Travel time/s	Saving time/s	Idling time/s	Total idle time/s	Saving idle time rate	Passing efficiency
Real	1900	–	24/40/94/30/73/40/75/117	493	–	55.56%
MIDM	1842	58	3/67/81	151	69.37%	83.33%
EVPS	1872	28	48	48	90.26%	94.44%

In comparison to the Real-based driving scenario, both MIDM and EVPS demonstrate a significantly reduced total driving time.

Regarding the frequency of stops at the signalized intersection, the velocity trajectory corresponding to the MIDM-based VPS is depicted in Fig. 11-(a). Here, it can be observed that there are six instances in which vehicles stop due to red lights at locations $L3_1$, $L3_3$, $L3_4$, $L3_6$, $L3_7$, and $L3_{10}$. The velocity trajectory associated with EVPS is presented in Fig. 11-(b). This method results in two stops at locations $L3_1$ and $L3_3$. The driving trajectories across three different VPSs along Route 3 are displayed in Fig. 11-(c). The trajectories generated by both MIDM-based and the EVPS exhibit similarities yet diverge from those derived from Real-based driving data. A significant interval exists between locations $L3_1$ and $L3_2$ during which driver maintains high speeds without access to forthcoming traffic information. After about 400 s, there are seven consecutive signals with uniform location distribution, and the velocity trajectories based on MIDM and EVPS are highly correlated to the Real-based driving in the case that the information of the signals ahead can be obtained.

The simulation results of the three VPS approaches at signalized intersections under Route 3 are presented in Table 8. Both MIDM-based and EVPS-based VPS exhibit significant reductions in travel time as well as total stopping time when contrasted with Real-based driving conditions. Specifically, under EVPS, there is a saving of approximately 196 s in driving time alongside 2 stops made during this period. This translates to a remarkable overall reduction of idle time by about 94.17%.

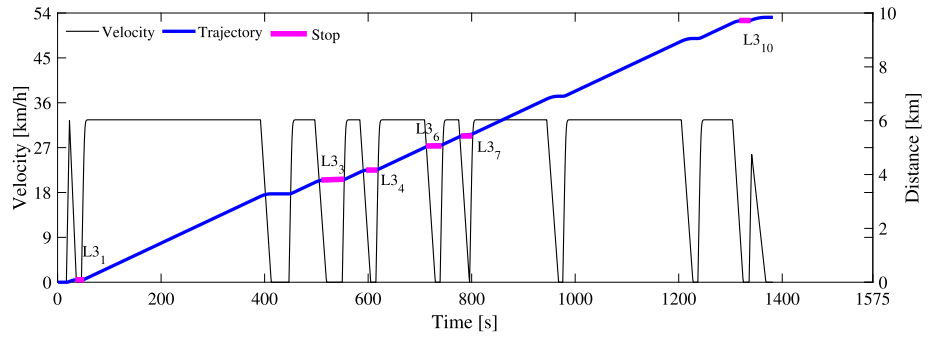

(a) MIDM-based driving

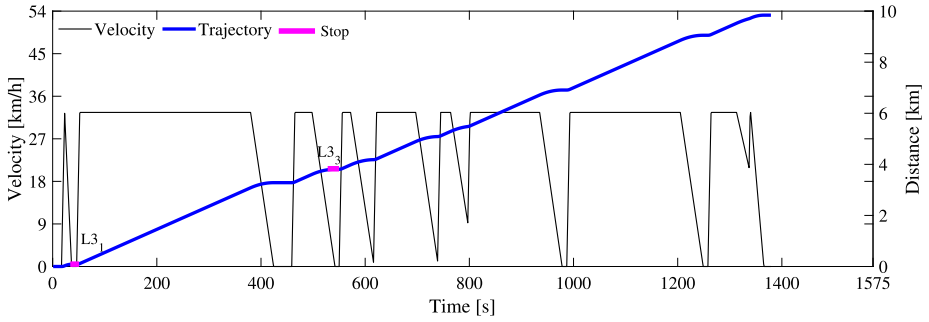

(b) EVPS-based driving

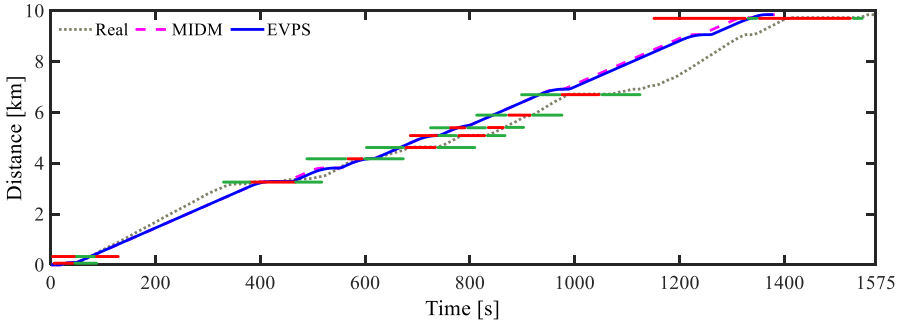

(c) Space-time trajectory for different VPSs

Fig. 11. Route 3: Trajectory of the FCHB.

Table 8
Route3: Results for three VPSs.

VPS	Travel time/s	Saving time/s	Idling time/s	Total idle time/s	Saving idle time rate	Passing efficiency
Real	1575	–	7/18/42/41/76/125	309	–	40.00%
MIDM	1382	193	10/31/11/10/1/10	73	76.38%	40.00%
EVPS	1379	196	10/8	18	94.17%	80.00%

In summary, these findings underscore the advantages offered by EVPS. The EVPS can reduce idling times at signalized intersections by more than 80.00% compared to Real-based driving practices. Furthermore, travel times across three routes are diminished by 42 s, 28 s, and 196 s, respectively, demonstrating robust adaptability.

5.1.4. Analysis of passing efficiency

We also analyze the characteristics associated with vehicle passage through signalized intersections utilizing identical velocity planning method across three distinct driving routes to gain deeper insights into how VPSs methods perform on varied roadways effectively. Traffic characteristics observed at intersections employing both MIDM-based VPS and EVPS-based method across these three routes are detailed in Table 9.

Table 9
Passage characterization based on the MIDM and EVPS.

Methods	Route	Travel time	Traffic light number	Idling times	Passing efficiency
MIDM	1	1667 s	8	2	75.00%
	2	1842 s	18	3	83.33%
	3	1382 s	10	6	40.00%
EVPS	1	1672 s	8	1	87.50%
	2	1872 s	18	1	94.44%
	3	1379 s	10	2	80.00%

The passing efficiency based on the MIDM is lowest in urban areas, followed by suburban and urban+suburban areas, respectively. The passing efficiency in urban areas is less than half of that observed in urban+suburban area, indicating that velocity control at signalized intersections could be enhanced. In contrast, the passing efficiency of the proposed EVPS across all three routes exceeds 80.00%, with a maximum recorded value of 94.44%. Notably, under this system, green

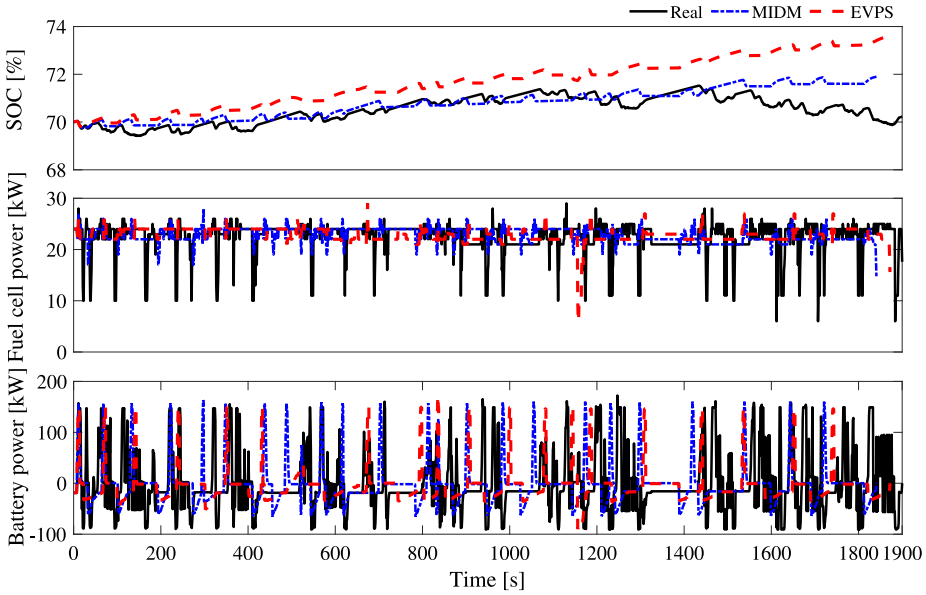

Fig. 12. Power output and SOC variation curves under Route 2.

lights facilitated smooth passage through 17 intersections. In summary, when compared to the Real-based driving and MIDM-based VPS, the proposed EVPS exhibits significant advantages regarding time savings, stopping duration, time savings rate, and overall passing efficiency.

5.2. The effectiveness of Q-learning-based EMS

5.2.1. FCHV's fuel economy

The velocity trajectories generated under the three VPSs serve as inputs for evaluating the effectiveness of a Q-learning-based EMS within varying operational conditions. Additionally, prior work related to EMS has been validated in Ref. [35] and will not be discussed further here.

For illustrative purposes, we consider an initial SOC set at 70%. Route 2, characterized by both suburban and urban road conditions, is selected for analysis. Corresponding SOC curves and power allocation modes derived from the Q-learning-based EMS across these three VPSs on Route 2 are presented in Fig. 12. It is observed that in Real-based driving scenarios, the final SOC is lower than those achieved with either MIDM-based VPS or EVPS approaches. Under EVPS operation, wherein fuel cells consistently function within their high-efficiency range, the power fluctuations in FCS and battery are minimized compared to those experienced under MIDM-based VPS conditions. Residual energy allows for battery charging via fuel cells which results in a higher SOC relative to both alternative methods.

Furthermore, DP-based EMS serves as a benchmark against which the performance of the proposed Q-learning-based EMS can be assessed concerning optimal FCHB power distribution strategies. Based on various combinations of VPS and EMS methods employed during simulations, six mdistinct approaches have been delineated, including EVPS+Q-learning, Real+Q-learning, MIDM+Q-learning, EVPS+DP, Real+DP, and MIDM+DP. Among these, the EVPS+Q-learning EMS represents the proposed cooperative approach. The variation of equivalent hydrogen consumption per 100 km under Route 2 is illustrated in Fig. 13. The highest equivalent hydrogen consumption per 100 km is observed with the Real+Q-learning method, followed by the Real+DP based method, MIDM+Q-learning, MIDM+DP, EVPS+Q-learning, and finally the lowest hydrogen consumption recorded under the EVPS+DP method.

The fuel economy across three routes is specifically detailed in Table 10. Overall, the equivalent hydrogen consumption per 100 km based on Real+Q-learning is found to be the highest among all three routes. In contrast, methods based on MIDM+Q-learning and EVPS+Q-learning demonstrate improvements exceeding 16.57% and 21.35%, respectively. Taking Route 2 as an example, when compared to both Real+Q-learning and MIDM+Q-learning methods, the proposed EVPS+Q-learning method achieves an equivalent hydrogen consumption of 4.09 kg per 100 km, resulting in savings of 29.85% and 15.15%, respectively. The equivalent hydrogen consumption of 100 km based on EVPS+Q-learning method is 0.12 kg more than that achieved by EVPS+DP method. Similarly, for the other two routes analyzed, are 0.19 kg and 0.18 kg more than that achieved by DP-based EMS. This indicates the Q-learning-based EMS effectively manages power distribution, yielding optimization outcomes that are 4.74%, 3.02%, and 4.80% lower than those achieved by DP-based EMS across all three routes, respectively.

Table 10
Results of the VPSs-based EMSs for three routes.

Route	Method	EMS	End value of SOC/%	Average efficiency of FCS/%	m_{100} /kg	Difference
1	Real	Q-learning	69.33	54.58	5.34	–
	MIDM	Q-learning	71.55	54.74	4.31	−19.29%
	EVPS	Q-learning	71.92	54.63	4.20	−21.35%
	Real	DP	70.00	54.30	5.11	−4.31%
	MIDM	DP	70.00	56.39	4.13	−22.66%
	EVPS	DP	70.00	56.46	4.01	−24.91%
2	Real	Q-learning	70.23	54.72	5.83	–
	MIDM	Q-learning	71.90	54.82	4.82	−17.32%
	EVPS	Q-learning	73.61	54.79	4.09	−29.85%
	Real	DP	70.00	55.10	5.55	−4.80%
	MIDM	DP	70.00	56.47	4.51	−22.64%
	EVPS	DP	70.00	56.37	3.97	−31.90%
3	Real	Q-learning	70.89	54.51	5.13	–
	MIDM	Q-learning	71.23	54.66	4.28	−16.57%
	EVPS	Q-learning	71.67	54.83	3.93	−23.39%
	Real	DP	70.00	56.48	4.98	−2.92%
	MIDM	DP	70.00	56.31	4.07	−20.67%
	EVPS	DP	70.00	56.54	3.75	−26.90%

m_{100} is the equivalent hydrogen consumption per 100 km.

5.2.2. FCS lifespan

During FCHB driving conditions, significant variability in fuel cell power can lead to reduced FCS lifespan. This variability under Q-learning-based EMS utilizing Real-based driving strategies alongside

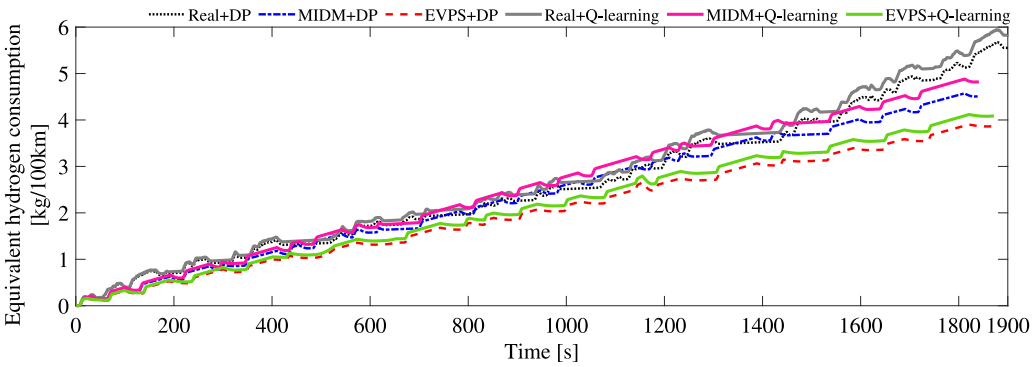

Fig. 13. Equivalent hydrogen consumption per 100 km for different strategies under Route 2.

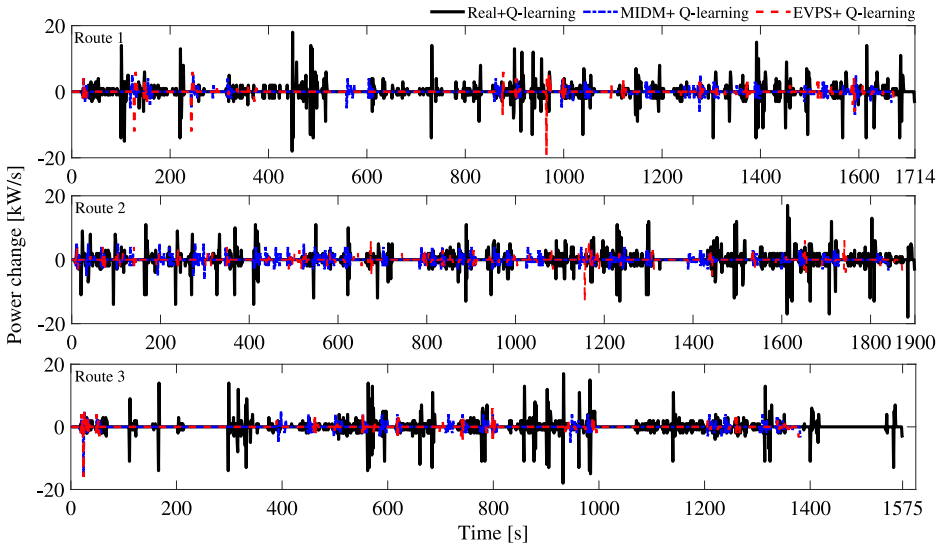

Fig. 14. Change rate of fuel cell power under three routes.

MIDM-based, and EVPS methods is depicted in Fig. 14. Notably frequent and substantial power fluctuations are observed with Real + Q-learning, where maximum fluctuation peaks at approximately 18 kW/s. The maximum rates of change reach up to about 6 kW/s under MIDM + Q-Learning. Changes associated with the proposed EVPS + Q-Learning exhibit considerably gentler variations.

The decay rates of the FCS for the three routes are presented in Table 11. In comparison to the decay rates observed under the Real+Q-learning and MIDM+Q-learning methods, the EVPS+Q-learning method demonstrates superior capabilities in power fluctuation smoothing and mitigation of severe operating condition. The results indicate that the proposed EVPS+Q-learning method achieves a relative reduction in decay rate by 39.55%, 46.15%, and 45.40% across three routes when compared to Real+Q-learning, highlighting its significant life enhancement effect.

Table 11
FCS decay under three routes with Q-learning-based EMS.

Route	Method	decay rate	Difference
1	Real	0.177‰	–
	MIDM	0.106‰	−40.11%
	EVPS	0.107‰	−39.55%
2	Real	0.208‰	–
	MIDM	0.114‰	−45.19%
	EVPS	0.112‰	46.15%
3	Real	0.163‰	–
	MIDM	0.090‰	−44.79%
	EVPS	0.089‰	−45.40%

5.3. Limitations

The EVPS proposed in this paper demonstrates the capability to reduce overall travel time, enhance the passing rate at intersections, and significantly decrease vehicle dwell time caused by signals when compared to real-world driving conditions. Furthermore, EVPS-based EMS can operate the fuel cell within its high-efficiency zone, offering substantial advantages in terms of fuel cell economy while also mitigating lifetime degradation.

However, it is important to note that this study does not account for vehicle jerk during travel when planning vehicle speed. This oversight results in elevated levels of jerk during certain travel phases, which adversely affects ride comfort. The variations in jerk associated with different speed strategies across three routes are illustrated in Fig. 15. It is evident that the jerks experienced under EVPS and MIDM across these three distinct routes exhibit a similar maximum fluctuation, which considerably compromises passenger comfort. Consequently, addressing this issue will be the main focus of future research efforts aimed at optimizing the VPS presented here.

6. Conclusion

This article presents an EVPS+Q-learning EMS designed to tackle challenges related to idling time, energy consumption, and FCS lifetime for demonstration FCHBs within urban transportation systems.

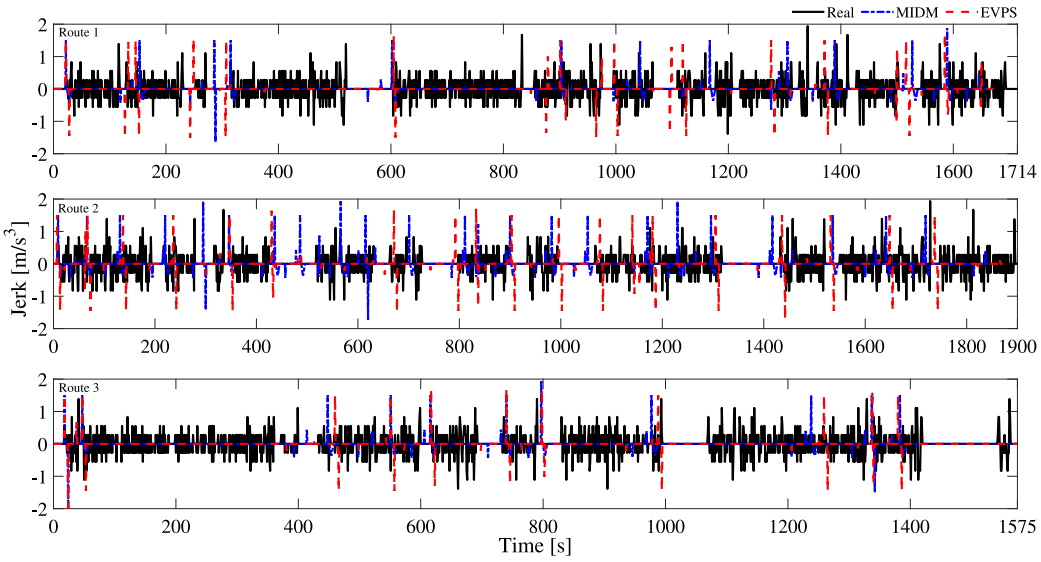

Fig. 15. Change rate of jerk under three routes.

Simulation results validate the effectiveness of this proposed approach in optimizing ecologically velocity profiles while minimizing adverse impacts associated with driving at signalized intersections, reducing energy consumption, and extending FCS lifespan. The methodology comprises three key components:

(1) An EVPS technique is introduced to compute optimal velocity profiles. This method effectively reduces waiting times at signalized intersections, achieving substantial improvements over strategies based on Real-based driving and MIDM-based VPS, respectively. Furthermore, its robustness has been confirmed.

(2) A Q-learning-based EMS is proposed to enhance FCS longevity while optimizing power distribution for a demonstration FCHB. Results reveal that the Q-learning-based EMS effectively manages power distribution, yielding optimization outcomes that are 4.74%, 3.02%, and 4.80% lower than those achieved by DP-based EMS across all three routes with EVPS, respectively.

(3) The proposed EVPS+Q-learning EMS presents a promising solution for enhancing fuel efficiency in FCHBs while simultaneously prolonging FCS lifetime in real time scenarios. It contributes significantly towards more sustainable and eco-friendly driving practices.

The authors anticipate exploring further avenues for future research: performance analysis across diverse SPAT information and road segments, consideration of dynamic traffic flow, and rigorous examination through hardware-in-the-loop simulation or field experimentation.

CRediT authorship contribution statement

Xiaohua Wu: Writing – review & editing, Supervision, Methodology, Funding acquisition. **Pengfei Ma:** Writing – original draft, Investigation. **Lingxue Zhou:** Writing – original draft, Software, Conceptualization. **Zhanfeng Fan:** Writing – review & editing, Conceptualization. **Qingbo Zhu:** Writing – review & editing, Methodology. **Xiaofeng Yin:** Supervision, Methodology, Conceptualization. **Quan Ouyang:** Writing – review & editing, Supervision.

Declaration of competing interest

The authors declare that they have no known competing financial interests or personal relationships that could have appeared to influence the work reported in this paper.

Acknowledgments

This work was supported by the National Natural Science Foundation of China (No. 52407254), the Science and Technology Department of Sichuan Province (No. 2024YFHZ0314), and the Industrial and Educational Integration Project of Yibin (No. YB-XHU-20240001).

Data availability

Data will be made available on request.

References

[1] Zhang B, Zhang J, Xu F, Shen T. Optimal control of power-split hybrid electric powertrains with minimization of energy consumption. Appl Energy 2020;266:114873. http://dx.doi.org/10.1016/j.apenergy.2020.114873.

[2] Shen Y, Cui P, Wang X, Han X, Wang Y. Variable structure battery-based fuel cell hybrid power system and its incremental fuzzy logic energy management strategy. Int J Hydrog Energy 2020;45(21):12130–42. http://dx.doi.org/10.1016/j.ijhydene.2020.02.083.

[3] Lu D, Yi F, Hu D, Li J, Yang Q, Wang J. Online optimization of energy management strategy for FCV control parameters considering dual power source lifespan decay synergy. Appl Energy 2023;348:121516. http://dx.doi.org/10.1016/j.apenergy.2023.121516.

[4] Jia C, Zhou J, He H, Li J, Wei Z, Li K, Shi M. A novel energy management strategy for hybrid electric bus with fuel cell health and battery thermal- and health-constrained awareness. Energy 2023;271:127105. http://dx.doi.org/10.1016/j.energy.2023.127105.

[5] Yu G, Li H, Wang Y, Chen P, Zhou B. A review on cooperative perception and control supported infrastructure-vehicle system. Green Energy Intell Transp 2022;1(3):100023. http://dx.doi.org/10.1016/j.geits.2022.100023.

[6] Li J, Wu X, Fan J, Liu Y, Xu M. Overcoming driving challenges in complex urban traffic: A multi-objective eco-driving strategy via safety model based reinforcement learning. Energy 2023;284:128517. http://dx.doi.org/10.1016/j.energy.2023.128517.

[7] Liu R, Liu H, Nie S, Han L, Yang N. A hierarchical eco-driving strategy for hybrid electric vehicles via vehicle-to-cloud connectivity. Energy 2023;281:128231. http://dx.doi.org/10.1016/j.energy.2023.128231.

[8] Li M, Wu X, He X, Yu G, Wang Y. An eco-driving system for electric vehicles with signal control under V2X environment. Transp Res C- Emerg Technol 2018;93:335–50. http://dx.doi.org/10.1016/j.trc.2018.06.002.

[9] Sun C, Guanetti J, Borrelli F, Moura SJ. Optimal eco-driving control of connected and autonomous vehicles through signalized intersections. IEEE Internet Things J 2020;7(5):3759–73. http://dx.doi.org/10.1109/jiot.2020.2968120.

[10] Zhang Y, Yuan W, Fu R, Wang C. Design of an energy-saving driving strategy for electric buses. IEEE Access 2019;7:157693–706. http://dx.doi.org/10.1109/access.2019.2950390.

[11] Guo L, Gao B, Gao Y, Chen H. Optimal energy management for HEVs in Eco-Driving applications using Bi-Level MPC. IEEE Trans Intell Transp Syst 2017;18(8):2153–62. http://dx.doi.org/10.1109/tits.2016.2634019.
[12] Wu Y, Tan H, Peng J, Zhang H, He H. Deep reinforcement learning of energy management with continuous control strategy and traffic information for a series-parallel plug-in hybrid electric bus. Appl Energy 2019;247:454–66. http://dx.doi.org/10.1016/j.apenergy.2019.04.021.
[13] Tang X, Zheng L, Chen J, Chen Z, Qin Y. Learning-based hierarchical cooperative eco-driving with traffic flow prediction for hybrid electric vehicles. Energy Convers Manage 2024;321:119000. http://dx.doi.org/10.1016/j.enconman.2024.119000.
[14] Yang D, Liu T, Song D, Zhang X, Zeng X. A real time multi-objective optimization guided-MPC strategy for power-split hybrid electric bus based on velocity prediction. Energy 2023;276:127583. http://dx.doi.org/10.1016/j.energy.2023.127583.
[15] Zhou H, Yu Z, Wu X, Fan Z, Yin X, Zhou L. Dynamic programming improved online fuzzy power distribution in a demonstration fuel cell hybrid bus. Energy 2023;284:128549. http://dx.doi.org/10.1016/j.energy.2023.128549.
[16] Wei X, Leng J, Sun C, Huo W, Ren Q, Sun F. Co-optimization method of speed planning and energy management for fuel cell vehicles through signalized intersections. J Power Sources 2022;518:230598. http://dx.doi.org/10.1016/j.jpowsour.2021.230598.
[17] Khalatbarisoltani A, Han J, Liu W, Hu X. Speedy hierarchical eco-planning for connected multi-stack fuel cell vehicles via health-conscious decentralized convex optimization. SAE Int J Electrified Veh 2024;13(1):129031. http://dx.doi.org/10.4271/14-13-01-0008.
[18] Khalatbarisoltani A, Boulon L, Hu X. Integrating model predictive control with federated reinforcement learning for decentralized energy management of fuel cell vehicles. IEEE Trans Intell Transp Syst 2023;24(12):13639–53. http://dx.doi.org/10.1109/TITS.2023.3303991.
[19] Chen W, Peng J, Ren T, Zhang H, He H, Ma C. Integrated velocity optimization and energy management for FCHEV: An eco-driving approach based on deep reinforcement learning. Energy Convers Manage 2023;296:117685. http://dx.doi.org/10.1016/j.enconman.2023.117685.
[20] Jia C, He H, Zhou J, Li J, Wei Z, Li K, Li M. A novel deep reinforcement learning-based predictive energy management for fuel cell buses integrating speed and passenger prediction. Int J Hydrog Energy 2025;100:456–65. http://dx.doi.org/10.1016/j.ijhydene.2024.12.338.
[21] Li K, Zhou J, Jia C, Yi F, Zhang C. Energy sources durability energy management for fuel cell hybrid electric bus based on deep reinforcement learning considering future terrain information. Int J Hydrog Energy 2024;52:821–33. http://dx.doi.org/10.1016/j.ijhydene.2023.05.311.
[22] Jia C, Zhou J, He H, Li J, Wei Z, Li K. Health-conscious deep reinforcement learning energy management for fuel cell buses integrating environmental and look-ahead road information. Energy 2024;290:130146. http://dx.doi.org/10.1016/j.energy.2023.130146.
[23] Yan M, Li G, Li M, He H, Xu H, Liu H. Hierarchical predictive energy management of fuel cell buses with launch control integrating traffic information. Energy Convers Manage 2022;256:115397. http://dx.doi.org/10.1016/j.enconman.2022.115397.
[24] Guo J, He H, Wei Z, Li J. An economic driving energy management strategy for the fuel cell bus. IEEE Trans Transp Electrif 2023;9(4):5074–84. http://dx.doi.org/10.1109/TTE.2022.3185215.
[25] Kim Y, Figueroa-Santos M, Prakash N, Baek S, Siegel JB, Rizzo DM. Co-optimization of speed trajectory and power management for a fuel-cell/battery electric vehicle. Appl Energy 2020;260:114254. http://dx.doi.org/10.1016/j.apenergy.2019.114254.
[26] Zhang L, Liao R, Wei X, Huang W. PMP method with a cooperative optimization algorithm considering speed planning and energy management for fuel cell vehicles. Int J Hydrog Energy 2024;79:434–47. http://dx.doi.org/10.1016/j.ijhydene.2024.06.297.
[27] Liu B, Sun C, Wang B, Liang W, Ren Q, Li J, Sun F. Bi-level convex optimization of eco-driving for connected fuel cell hybrid electric vehicles through signalized intersections. Energy 2022;252:123956. http://dx.doi.org/10.1016/j.energy.2022.123956.
[28] Liu C, Chen Y, Xu R, Ruan H, Wang C, Li X. Co-optimization of energy management and eco-driving considering fuel cell degradation via improved hierarchical model predictive control. Green Energy Intell Transp 2024;3(6):100176. http://dx.doi.org/10.1016/j.geits.2024.100176.
[29] Zhou J, Peng J, Wu J, Wei Z, Fan Y, Guo X. Multi-performance enhanced eco-driving strategy for connected fuel cell hybrid electric bus based on stein soft actor-3-critic. Energy 2024;307:132697. http://dx.doi.org/10.1016/j.energy.2024.132697.
[30] Yan M, Xu H, Li M, He H, Bai Y. Hierarchical predictive energy management strategy for fuel cell buses entering bus stops scenario. Green Energy Intell Transp 2023;2(4):100095. http://dx.doi.org/10.1016/j.geits.2023.100095.
[31] Li M, Yin L, Yan M, Wu J, He H, Jia C. Hierarchical intelligent energy-saving control strategy for fuel cell hybrid electric buses based on traffic flow predictions. Energy 2024;304:132144. http://dx.doi.org/10.1016/j.energy.2024.132144.
[32] Dong H, Chen H, Zhou Y, Li Z, Yin G, Zhuang W. Velocity optimization of connected electric vehicle at multiple signalized intersections for energy efficiency and traffic throughput improvement. In: 2021 6th international conference on transportation information and safety. ICTIS, 2021, p. 1004–9. http://dx.doi.org/10.1109/ICTIS54573.2021.9798558.
[33] Hu L, Zhong Y, Hao W, Moghimi B, Huang J, Zhang X, Du R. Optimal route algorithm considering traffic light and energy consumption. IEEE Access 2018;6:59695–704. http://dx.doi.org/10.1109/access.2018.2871843.
[34] Li W, Ye J, Cui Y, Kim N, Cha SW, Zheng C. A speedy reinforcement learning-based energy management strategy for fuel cell hybrid vehicles considering fuel cell system lifetime. Int J Precis Eng Manuf Green Technol 2022;9(3):859–72. http://dx.doi.org/10.1007/s40684-021-00379-8.
[35] Deng P, Wu X, Yang J, Yang G, Jiang P, Yang J, Bian X. Optimal online energy management strategy of a fuel cell hybrid bus via reinforcement learning. Energy Convers Manage 2024;300:117921. http://dx.doi.org/10.1016/j.enconman.2023.117921.